

A Convex Approximation for the Tertiary Control of Unbalanced Microgrids.

Diego-Alejandro Ramirez^{a,*}, Alejandro Garcés^b, Juan-José Mora-Flórez^b

^a*XM S.A. E.S.P, Cl. 12 Sur N18-168, Medellín, Colombia*

^b*Department of electric power systems engineering. Universidad Tecnológica de Pereira. AA: 97 - Post Code: 660003 - Pereira, Colombia*

Abstract

This article presents an optimization model for tertiary control in three-phase unbalanced microgrids. This model considers 24h operation and includes renewable energy sources, energy storage devices, and grid code limitations. Power flow equations are simplified using a recently developed approximation based on Wirtinger's calculus. The proposed model is evaluated both theoretically and practically. From the theoretical point of view, the model is suitable for tertiary control since it is convex; hence, global optimum, uniqueness of the solution, and convergence of the interior point method are guaranteed. From the practical point of view, the model is simple enough to be implemented in a small single-board computer with low time calculation. The latter is evaluated by implementing the model in a Raspberry-Pi board with the CIGRE low voltage benchmark; the model is also evaluated in the IEEE 123-nodes test system for power distribution networks.

Keywords: Tertiary control, Optimal power flow, convex optimization, Wirtinger calculus, linear power flow.

1. Introduction

1.1. Motivation

Modern power distribution systems include distributed resources like wind and solar generation as well as storage devices. These components can be grouped, forming a microgrid with potential improvements in efficiency and reliability. However, to achieve these improvements, a microgrid must be complemented with an optimization algorithm called tertiary control, which will be referred to as TC in the rest of the paper [1].

An optimization model for TC requires to include constraints related to renewable energies and energy storage devices and an accurate representation of the power flow equations. Besides, the model must be tailored for real implementation. Therefore, it is convenient to formulate a model that guarantees global optimum, uniqueness of the solution, and convergence of the algorithms. Convex optimization emerges as a suitable alternative in this context. Nevertheless, the power flow equations introduce non-convex constraints that require linearization, considering a trade-off between precision and convexity [2]. On the other hand, the model must be simple enough to be implemented in a practical situation, with a well-defined time frame for the entire process, and considering time calculations and latency of the communications [3].

1.2. State of the art

TC is the highest level in the hierarchy for microgrids operation [4]. It defines the optimal operation point for the active and reactive power in each distributed resource and how much energy the microgrid is willing to trade with the primary grid to satisfy the power balance between the load and power generation [5].

The problem is closely related to the optimal power flow and the management of energy storage devices. The optimal power flow is a classic problem that has regained importance due to the challenges associated with introducing renewable energy and new advances in convex optimization [6]. A modern approach to this problem is based

*Corresponding author

Email addresses: dramirez@xm.com.co (Diego-Alejandro Ramirez), alejandro.garcés@utp.edu.co (Alejandro Garcés), jjmora@utp.edu.co (Juan-José Mora-Flórez)

Table 1: Aspects considered in recent references about tertiary control for microgrids.

Aspect Reference	Conic relaxations [6] to [9]	Heuristics [11] to [12]	AI [15] to [16]	Energy Management [17] to [19]	Proposed approach
Convergence guarantee	●	○	◐	○	●
Global optimum	●	◐	◐	○	●
Energy storage	○	○	○	●	●
Practical oriented	◐	○	●	◐	●
Implementation	○	○	○	○	●
Stochastic model	○	○	○	●	◐

on conic approximations such as semidefinite programming and second-order cone optimization (see [7] and the references therein for a complete review of this subject). These relaxations transform the non-convex problem into a convex thereof with theoretical and practical advantages related to global optimal, uniqueness of the solution, and fast convergence rate [8]. Despite obvious theoretical advances, these algorithms are far from becoming a proper tertiary control in practical applications [9]. Computational time may be high, especially in semidefinite approximations, and its implementation may require solvers that allow conic programming [10]. In addition, the algorithms should be tailored to be implemented in low-cost single-board computers and not in a desktop computer.

Another classic approach for the optimal power flow problem is using heuristic algorithms [11]. These algorithms have an extensive history in power systems applications, especially in planning problems. However, they are not suitable for real-time operation problems. Computational time is cumbersome in these algorithms, and convergence is not guaranteed [12]. Besides, the abuse of heuristic analogies in optimization problems has been criticized in the scientific community [13]. Other methods based on artificial intelligence have also been proposed, especially reinforcement learning [14] and neural networks [15]. These types of algorithms are promising for real-time implementation, although they may be improved by theoretical analysis of the optimization problem [16].

TC must consider power flow constraints and energy management of both renewable generation and energy storage resources [17]. This aspect is usually studied under the name of energy storage management [18]. The problem may allow 24h operation but tends to neglect the network effects. The stochastic nature of the problem has been also studied [19] in both the optimal power flow and the energy management problems.

1.3. Contribution

This paper presents a model based on a linearization recently proposed in [20]. The contribution of the article can be summarized as follows:

- An optimization model for 24h operation, considering unbalanced operation, realistic models of the loads and, renewable and storage devices.
- A convex approximation of the batteries losses and the exponential models of loads (previous linearizations considered constant impedance, current, and power, known as ZIP models and did not consider the non-linear model of the batteries).
- A static reserve model that allows the transition from grid-connected to island operation.
- An implementation in a small single-board computer (a Raspberry Pi) that demonstrates the proposed algorithm can be implemented in practice at a low cost.

Table 1 shows a comparison with recent references, considering the main aspects for TC in microgrids. ● indicates an aspect that was fully considered in the reference, ◐ indicates an aspect that was partially considered, and ○ indicates an aspect that was not considered in said reference.

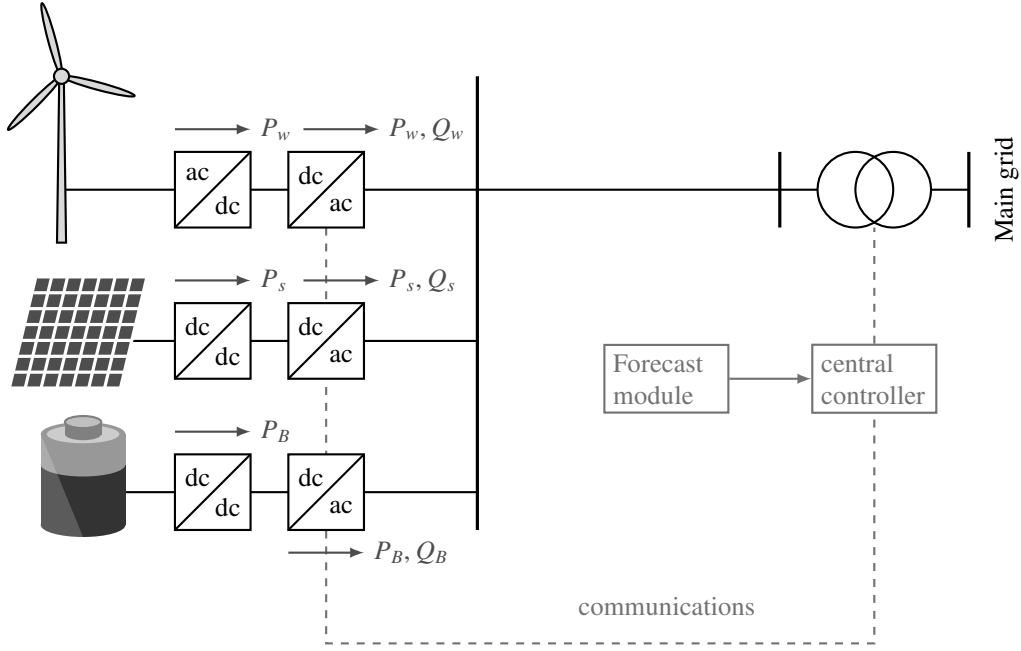


Figure 1: Integration of wind, solar and energy storage devices through power electronic converters, including TC.

1.4. Organization of the paper

The paper is organized as follows: Section 2 shows the architecture of the proposed TC. A general representation of three-phase microgrids and their main components, such as wind turbines, solar panels, and energy storage devices, is presented in Section 3. Next, a general formulation of the power flow equations for grid-connected operation is presented in Section 4. The proposed Wirtinger linearization is described in Section 5, resulting in a convex model. The CIGRE microgrid benchmark results are presented in Section 6, followed by its software implementation. Finally, conclusions and recent references are presented.

2. Tertiary control in microgrids

Microgrids are usually operated using a hierarchical control that emulates the automatic generation control of conventional power systems. This hierarchy consists of three controls known as primary, secondary, and tertiary control. Primary control aims to synchronize and stabilize the microgrid, while secondary control aims to achieve nominal frequency; finally, tertiary control aims to optimize the operation. Therefore, TC operates in a stationary or quasi-stationary state.

A typical architecture for TC is shown in Figure 1. Renewable resources and energy storage devices are integrated through power electronics converters to control active and reactive power. However, this control is limited by the converters' capacity and the primary resource availability (i.e., solar irradiance and wind speed). Besides, the state of charge of the batteries (SOC) must be managed to minimize power loss and/or reduce costs. Therefore, an optimization problem requires to be executed by a central controller in real-time.

Real-time may mean different things, according to the application. For a primary control, real-time is an action executed in the order of seconds or even milliseconds, whereas for the tertiary control, real-time is in the order of minutes. The tertiary control is, therefore, a quasi-dynamic model that works in an entire day.

Different types of communications technologies can be used in this architecture, for example, WiFi or ZigBee [21]. In any case, delays or latency must be considered; these delays include those associated with the optimization model and those associated with the communications. The maximum latency experienced by the ZigBee technology for a distance of 50 m with 50-byte packets was 18 ms, according to [22]. Therefore, the primary source of delay is the execution time of the optimization model. Therefore, fast algorithms with convergence guaranteed are required.

The central controller can be any device, such as a personal computer or an industrial computer; however, it is advisable an embedded system dedicated explicitly for TC. This system must be small and reliable to be placed in the point of common coupling, that is, the point where the microgrid is electrically connected to the electric distribution system. The optimization model requires to be accurate but straightforward enough to be implemented in this device. This is the main objective of the model presented in the next section.

3. Modelling

Nomenclature			
α_k	Exponential model of load k	$I_{\mathcal{H}}$	Vector of nodal currents
\circ	Hadamard product	n_{kt}^{char}	Losses in the energy storage during charging
\mathbb{I}_3	Identity matrix of size 3×3	n_{kt}^{disch}	Losses in the energy storage during discharging
\mathcal{E}	Set of three-phase branches (hyperbranches)	p_{kt}^{char}	Power in the battery during charging
\mathcal{H}	Set of three-phase nodes (hypernodes)	p_{kt}^{disch}	Power in the battery during discharging
\mathcal{N}	Hypernodes different from slack, i.e $\mathcal{N} = \mathcal{H} - \mathcal{S}$	p_t^{grid}	Total power supplied for the main grid at time t
\mathcal{S}	Slack hypernode	p_t^{loss}	Total power loss at time t
\otimes	Kronecker product	s_{kt}	Apparent power in node k at time t
∂	Conventional derivative	s_{kt}^{solar}	Power generated by photovoltaic unit k at time t
ψ_t	Irradiance at time t	s_{kt}^{wind}	Power generated by wind turbine k at time t
ρ_k	Productivity coefficient associated with the solar panel k	v^{nom}	Nominal phase-to-neutral voltage
$\widehat{\partial}$	Wirtinger's derivative	$V_{\mathcal{E}}$	Vector of branch voltages
A	Node-branch incidence matrix	$V_{\mathcal{H}}$	Vector of nodal voltages
e_{kt}	Energy in the battery k at time t	w_t	wind speed at time t
e_{kt}	Energy stored in the battery k at time t	$Y_{\mathcal{H}}$	Three-phase admittance matrix
$I_{\mathcal{E}}$	Vector of branch currents		

3.1. Three-phase grid

A three-phase microgrid is represented as a connected hypergraph $\mathcal{G} = \{\mathcal{H}, \mathcal{E}\}$, where \mathcal{H} represents the set of hypernodes and $\mathcal{E} \subseteq \mathcal{N} \times \mathcal{N}$ represents the hyperbranches. Each hypernode and hyperbranch has three components that represent phases $\{A, B, C\}$ as depicted in Fig 2. Along this section and for the rest of the paper, matrices and vectors are represented in capital letter whereas entries of these matrices/vectors are represented in lower case letters. Unless otherwise specified, all variables are defined in the complex domain; \bar{x} represents the complex conjugate of x , and X^T is the conjugate transpose of X . Subscripts represent node and/or time whereas superscripts represent labels of the variables, if they are text, and, exponentiation if they are numeric.

Circuit variables in each hyperbranch $l \in \mathcal{E}$ are represented by a 3×3 admittance matrix as given in (1).

$$I_l = Y_l V_l \quad (1)$$

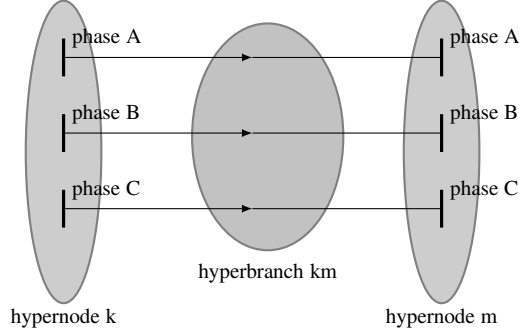


Figure 2: Hypergraph representation for line sections in microgrids

These matrices can be grouped together in a block diagonal matrix $Y_{\mathcal{E}}$ that relates the vector of three-phase voltages with the vector of three-phase currents, as given in (2).

$$I_{\mathcal{E}} = Y_{\mathcal{E}}V_{\mathcal{E}} \quad (2)$$

where $V_{\mathcal{E}}$ and $I_{\mathcal{E}}$ are vectors where the first elements correspond to the phase A, next the phase B and finally the phase C. An incidence matrix $A \in \mathbb{R}^{\mathcal{H} \times \mathcal{E}}$ is created for the hypergraph, where $a_{kl} = 1$ if the hyperbranch $l \in \mathcal{E}$ is in the direction $k \rightarrow m$ and $a_{kl} = -1$ if it is in the direction $m \rightarrow k$. The other entries of the matrix are zero. This matrix requires to be increased in order to consider three phases in each hypernode. Therefore, the following expressions are obtained:

$$I_{\mathcal{H}} = (\mathbb{I}_3 \otimes A)I_{\mathcal{E}} \quad (3)$$

$$V_{\mathcal{E}} = (\mathbb{I}_3 \otimes A)^{\top}V_{\mathcal{H}} \quad (4)$$

$$I_{\mathcal{H}} = (\mathbb{I}_3 \otimes A)Y_{\mathcal{E}}((\mathbb{I}_3 \otimes A))^{\top}V_{\mathcal{H}} = Y_{\mathcal{H}}V_{\mathcal{H}} \quad (5)$$

where \mathbb{I}_3 is the identity matrix of size 3×3 , $Y_{\mathcal{H}}$ is the three-phase admittance matrix, \otimes is the Kronecker product and $(\cdot)^{\top}$ represents the transpose conjugate.

The hypernode set is divided in two new sets $\mathcal{H} = \{\mathcal{S}, \mathcal{N}\}$ where \mathcal{S} represents the slack hypernode and \mathcal{N} are the rest of hypernodes. Therefore, the model of the grid is given by the following matrix equations:

$$I_{\mathcal{S}} = Y_{\mathcal{S}\mathcal{S}}V_{\mathcal{S}} + Y_{\mathcal{S}\mathcal{N}}V_{\mathcal{N}} \quad (6)$$

$$I_{\mathcal{N}} = Y_{\mathcal{N}\mathcal{S}}V_{\mathcal{S}} + Y_{\mathcal{N}\mathcal{N}}V_{\mathcal{N}} \quad (7)$$

where

$$Y_{\mathcal{H}} = \begin{pmatrix} Y_{\mathcal{S}\mathcal{S}} & Y_{\mathcal{S}\mathcal{N}} \\ Y_{\mathcal{N}\mathcal{S}} & Y_{\mathcal{N}\mathcal{N}} \end{pmatrix} \quad (8)$$

Notice that \mathcal{S} is size three since there are three slack nodes in the system, corresponding to each phase. The voltage $V_{\mathcal{S}}$ is given by (9):

$$V_{\mathcal{S}} = v^{\text{nom}} \begin{pmatrix} 1 \\ e^{-2\pi/3j} \\ e^{2\pi/3j} \end{pmatrix} \quad (9)$$

where v^{nom} is the nominal voltage in per unit, measured in the point of point of common coupling. On the other hand, voltages $V_{\mathcal{N}}$ are variables in the optimization model and thus, the current in each node of the grid is in function of these voltages

$$i_k = \sum_{s \in \mathcal{S}} y_{sk}v_s + \sum_{m \in \mathcal{N}} y_{km}v_m, \quad \forall k \in \mathcal{N} \quad (10)$$

multiplying by \bar{v}_k an expression for the nodal powers is obtained as follows:

$$\bar{s}_{kt} = \sum_{m \in \mathcal{S}} \bar{v}_{kt}y_{mk}v_{mt} + \sum_{m \in \mathcal{N}} \bar{v}_{kt}y_{km}v_{mt}, \quad \forall k \in \mathcal{N} \quad (11)$$

where \bar{v}_k represents the complex conjugate of v_k and $s_k = p_k + jq_k$ is the total apparent power in node k . A subscript t was added to all variables to indicate the time since the model is formulated for one day operation.

Each node may have different power injections such as wind and solar generation, energy storage and, loads. Therefore, the following balance of power in each node is obtained:

$$s_{kt} = s_{kt}^{\text{wind}} + s_{kt}^{\text{solar}} + s_{kt}^{\text{battery}} - s_{kt}^{\text{load}} \quad (12)$$

Total losses of the grid are calculated as given in (13).

$$p_t^{\text{loss}} = \text{real} \left(V_{S_t}^\top Y_{SS} V_{S_t} + 2V_{S_t}^\top Y_{SN} V_{N_t} + V_{N_t}^\top Y_{NN} V_{N_t} \right) \quad (13)$$

Further, the power supplied by the main grid to the microgrid is defined as follows

$$p_t^{\text{grid}} = \text{real} \left((Y_{SS} V_{S_t} + Y_{SN} V_{N_t})^\top V_{S_t} \right) \quad (14)$$

This variable defines the interchange of power with the main grid, and hence, it is essential for the optimization model.

3.2. Three-phase exponential load model

Three-phase loads are represented by a general model that considers constant power, constant current, and constant impedance [23]. This model can be described in terms of a constant $\alpha \in \{0, 1, 2\}$ as given in (15) where 0 corresponds to constant power, 1 to constant current and 2 to constant impedance. Fractional values of α_k are also allowed in the model.

$$s_{kt}^{\text{load}} = s_{kt}^{\text{ZIP}} \left\| \frac{V_{kt}}{V_{\text{nom}}} \right\|^{\alpha_k} \quad (15)$$

A time series for s_k^{load} is required in order to obtain the 24h operation.

3.3. Photovoltaic units

The model that represents the power supplied by the photovoltaic units (PVs) during a period is presented in (16)

$$p_{kt}^{\text{solar}} \leq \rho_k \psi_t \quad (16)$$

where p_{kt}^{solar} power that the photovoltaic generator can inject in the period t , ρ_k is the productivity coefficient associated to the solar panel, and ψ_t corresponds to the irradiance measured in (W/m^2), perpendicular to the panel for the period t . The model requires a time series of ψ for 24 h. Power electronic converters are allowed to reduce their production if required by the optimization model there in the inequality.

3.4. Wind turbine model

Generally, a model for the generated wind power may be obtained using a wind turbine profile obtained experimentally. In this case, the proposed model represents an approximation of the active power supplied by the wind turbine; thus the wind power may be calculated based on the wind speed and the wind turbine power coefficient as follows:

$$p_{kt}^{\text{wind}} \leq \left\{ \begin{array}{ll} p_k^{\text{nom}} \left(\frac{w_t}{w_k^{\text{nom}}} \right)^3, & \text{if } 0 \leq w_t \leq w_k^{\text{nom}} \\ p_k^{\text{nom}}, & \text{if } w_k^{\text{nom}} \leq w_t \leq w_k^{\text{max}} \\ 0, & \text{if } w_k^{\text{max}} \leq w_t \end{array} \right\} \quad (17)$$

where p_{kt}^{wind} corresponds to the maximum power that the wind turbine can deliver in the period of time t , the wind speed is a time variable described by w_t , and p_k^{nom} is the rated power that each of the wind turbines can inject to the system. w_k^{nom} represents the rated wind speed at which the turbines generate its rated power, and the maximum wind speed that the turbines tolerates is represented by w_k^{max} . The model requires a time series of the wind velocity during a period of time.

3.5. Battery energy storage

The following equation proposes a simplified dynamic model of the battery energy storage k at each time t .

$$e_{kt} = e_{kt-1} + (p_{kt}^{\text{char}} - p_{kt}^{\text{disch}}) \Delta t \quad (18)$$

where p_{kt}^{char} is the charging power, p_{kt}^{disch} is the power at discharge, and e_{kt} is the energy stored by the batteries, considering a positive value if it injects power to the microgrid and a negative value for the charging mode. Δt is the time discretization (usually 1h). A quadratic model of the losses in the battery and the converter is proposed, considering efficiencies of charge and discharge as follows:

$$n_{kt}^{\text{char}} = a_k^{\text{char}} (p_{kt}^{\text{char}})^2 + b_k^{\text{char}} p_{kt}^{\text{char}} + c_k^{\text{char}} \quad (19)$$

$$n_{kt}^{\text{disch}} = a_k^{\text{disch}} (p_{kt}^{\text{disch}})^2 + b_k^{\text{disch}} p_{kt}^{\text{disch}} + c_k^{\text{disch}} \quad (20)$$

this model is taken from data-sheets of batteries (see for example [24]). It is important to remark that a^{charge} and $a^{\text{discharge}}$ are always positive. Then, the active power delivered by the battery energy storage is given by the following equations:

$$p_{kt}^{\text{char}} - p_{kt}^{\text{disch}} = \text{real}(s^{\text{battery}}) \quad (21)$$

3.6. Power and voltage limits

Photovoltaic units, wind turbines, and battery energy storage devices are integrated into the microgrid through power electronic converters, as depicted in Fig 1. These converters can generate or consume reactive power on the assumption that the current and apparent power is below its maximum.

Therefore, the apparent power is limited by the following constrain:

$$\|s_k^{\text{device}}\| \leq s_{\text{max}}^{\text{device}}, \quad \forall \text{device} \in \{\text{wind, solar, battery}\} \quad (22)$$

Notice that this constraint is convex.

On the other hand, voltage limits are considered by the following constraint:

$$\|v_k - v^{\text{nom}}\| \leq \delta v^{\text{nom}} \quad (23)$$

where δ is the maximum voltage deviation according to the grid code.

3.7. Static reserve

A *static reserve* is proposed in the model. This new concept is strongly related to the energy stored by the batteries. It is applied because it needs to keep the system secure and in equilibrium when the system changes from grid-connected to island operation. The static reserve guarantees a time of safe operation in which the demand of the microgrid can be supplied by the available generation and energy stored by the batteries. Taking this criterion into account, a deficit d_t of power provided by generators is defined as a function of the demand and the power injected by the slack node to the microgrid as given in (24),

$$d_t = \sum_{k \in \mathcal{N}} s_k^{\text{load}} - p_t^{\text{grid}} \quad (24)$$

Therefore, the energy stored by the batteries is limited by the following constraints:

$$\sum_{k \in \mathcal{N}^{\text{battery}}} e_{kt} \geq \text{real}(d_t) \quad (25)$$

Where $\mathcal{N}^{\text{battery}} \subseteq \mathcal{N}$ is the subset of nodes that have battery energy storage.

4. Optimization problem

The proposed power flow requires a time series for wind speed, solar irradiance, and power demand. The optimization model search for optimal use of energy storage devices as given below, where all variables depend on the time, and therefore, the subindex t is omitted in most of the equations.

The model seeks to minimize the costs c_t of the energy supplied by the primary grid. The model of each component and the grid itself are also considered. For the sake of completeness, the entire model is presented in Table 2 including the type of equation (notice that quadratic equality constraints are also non-convex).

Table 2: Non-convex model for the tertiary control (NC-TC Model)

Equation	Type	Characteristic
$\min \sum_t c_t p_t^{\text{grid}}$	objective function	affine
(11)	load flow	non-convex
(12)	power balance	affine
(13)	power loss	quadratic equality
(14)	grid power	quadratic equality
(15)	load model	non-convex
(16)	solar generation	affine
(17)	wind generation	affine
(18)	energy balance	affine
(19)	battery charging	quadratic equality
(20)	battery discharge	quadratic equality
(21)	battery power	affine
(22)	converter capacity	second-order cone
(23)	voltage limits	second-order cone
(24)	power deficit	affine
(25)	static reserve	affine

The model presented in Table 2 is called, in this paper, as non-convex tertiary control model (hereafter called NC-TC Model). This model contains some complex variables (e.g. s_k, v_k and v_m) which simplifies its representation. However, it is important to remark that this is only a representation since an optimization model requires to be defined in an ordered set (for example, the set \mathbb{R}^n). Therefore, each equality constraint with complex variables must be separated into real and imaginary parts. This complex representation allows a simple formulation of the linearizations using Wirtinger's calculus. The resulting linearizations can be written directly in complex form, in packages such as *cvxpy* as explained in the next section.

4.1. Convex identification

NC-TC model is non-linear and non-convex, and therefore, a convex approximation is required. However, some parts of the model are already convex, for instance, affine equations. Power loss, grid power, and loss in the battery energy storage devices are all quadratic equality constraints. These equations define, in principle, non-convex sets. However, they can be transformed into convex sets by replacing equality for inequality constraints and noticing that these quadratic forms are all convex. This approximation is suitable since the objective function includes minimizing p^{grid} and hence, the inequality gap tends to be minimized.

The only remaining non-convex constraints are (11) and (15). These constraints will be linearized by using Wirtinger calculus as presented in the next subsection.

5. Convex model

5.1. Wirtinger's linearization

In general, an equality constraint is non-convex unless it is an affine equation. Therefore, a linearization is recommended in order to approximate the model to a convex set.

Let us consider a complex variable $z = x + jy$ and a complex function $f(z) = u + jv$. The Wirtinger's derivate and the conjugate Wirtinger's derivate are defined as follows:

$$\frac{\widehat{\partial}f}{\partial z} = \frac{1}{2} \left(\frac{\partial u}{\partial x} + \frac{\partial v}{\partial y} \right) + \frac{j}{2} \left(\frac{\partial v}{\partial x} - \frac{\partial u}{\partial y} \right) \quad (26)$$

$$\frac{\widehat{\partial}f}{\partial \bar{z}} = \frac{1}{2} \left(\frac{\partial u}{\partial x} - \frac{\partial v}{\partial y} \right) + \frac{j}{2} \left(\frac{\partial v}{\partial x} + \frac{\partial u}{\partial y} \right) \quad (27)$$

These operators are very similar to the conventional derivatives, despite the fact that they are not derivatives in the Cauchy-Riemann sense (see [25] and [26] for more details). More importantly, these operators allow a linearization on the complex numbers for non-holomorphic functions such as (11) and (15).

A complex function linearization in terms of the Wirtinger's operators is defined as follows:

$$f \approx f(z_0) + \frac{\widehat{\partial}f}{\partial z} \Delta z + \frac{\widehat{\partial}f}{\partial \bar{z}} \Delta \bar{z} \quad (28)$$

For example, a function $f = \bar{v}_k v_m$ can be linearized around a point v_{k0}, v_{m0} as follows:

$$f(\bar{v}_k, v_m) = \bar{v}_k v_m \quad (29)$$

$$\approx \bar{v}_{k0} v_{m0} + v_{m0} \Delta \bar{v}_k + \bar{v}_{k0} \Delta v_m \quad (30)$$

$$= \bar{v}_{k0} v_{m0} + v_{m0} (\bar{v}_k - \bar{v}_{k0}) + \bar{v}_{k0} (v_m - v_{m0}) \quad (31)$$

$$= v_{m0} \bar{v}_k + \bar{v}_{k0} v_m - \bar{v}_{k0} v_{m0} \quad (32)$$

Notice that Wirtinger's derivatives fulfill the basic properties for differentiation known from real-valued analysis concerning the linearity, product rule and composition of functions.

5.2. Wirtinger's Linearization of the power flow equations

The linearization presented in (32) can be used for linearizing (11), as follows:

$$\bar{s}_{kt} = \sum_{m \in \mathcal{S}} \bar{v}_{kt} y_{mk} v_{mt} + \sum_{m \in \mathcal{N}} y_{km} (v_{m0} \bar{v}_k + \bar{v}_{k0} v_m - \bar{v}_{k0} v_{m0}) \quad (33)$$

After simple algebraic manipulations the following matrix representation is obtained:

$$\begin{aligned} \bar{S}_{Nt} &= \text{diag}(Y_S \cdot V_{St}) \cdot \bar{V}_{Nt} + \text{diag}(Y_N \cdot V_{N0}) \cdot \bar{V}_{Nt} + \\ &\quad (\text{diag}(\bar{V}_{N0}) \cdot Y_N) \cdot V_{Nt} - \text{diag}(V_{N0}) \cdot (Y_N \cdot \bar{V}_{N0}) \end{aligned} \quad (34)$$

Equation (34) defines an affine space which constitutes an approximation of the power flow. The following matrices are defined in order to simplify the nomenclature:

$$K = \text{diag}(Y_S V_S) + \text{diag}(Y_N \cdot V_{N0}) \quad (35)$$

$$L = \text{diag}(\bar{V}_{N0}) \cdot Y_N \quad (36)$$

$$U = -\text{diag}(V_{N0}) \cdot (Y_N \cdot \bar{V}_{N0}) \quad (37)$$

Therefore, Constraint (11) is transformed into the following affine equation:

$$\bar{S}_{Nt} = K \cdot \bar{V}_{Nt} + L \cdot V_{Nt} + U \quad (38)$$

Precision of this approximation was evaluated in [20], where results demonstrated errors less than 1×10^{-3} in voltages. It is important to remark that the linearization is defined in the complex domain, therefore, v_{k0} must consider the phase (i.e., e^{0j} for phase A, $e^{-2\pi/3j}$ for phase B and $e^{2\pi/3j}$ for phase C).

5.3. Wirtinger's linearization for exponential loads

Equation (15) can be also linearized using Wirtinger's calculus. The non-linear term in this expression is given by (39).

$$\|v_k\|^\alpha = (v_k \bar{v}_k)^{\frac{\alpha}{2}} \quad (39)$$

Linearizing around v_{k0} the following expression is obtained

$$\begin{aligned} (v_k \bar{v}_k)^{\frac{\alpha}{2}} &\approx (v_{k0} \bar{v}_{k0})^{\frac{\alpha}{2}} + \frac{\widehat{\partial} \|v_k\|^\alpha}{\partial v_k} \Delta v_k + \frac{\widehat{\partial} \|v_k\|^\alpha}{\partial \bar{v}_k} \Delta \bar{v}_k \\ &= (v_{k0} v_{k0}^*)^{\frac{\alpha}{2}} + \frac{\alpha}{2} (v_{k0} \bar{v}_{k0})^{\frac{\alpha}{2}-1} (\bar{v}_{k0} \Delta v_k + v_{k0} \Delta \bar{v}_k) \end{aligned} \quad (40)$$

Considering that the voltages of the system are near of the nominal value, a good point of linearization is $v_{k0} = v^{\text{nom}} e^{j\phi}$ as the complex nominal voltage, where ϕ is 0, $-\pi/3$ or $\pi/3$ according to the phase. Therefore, the nonlinearity of the ZIP load model is represented linearly by the following expression:

$$\begin{aligned} (v_k \bar{v}_k)^{\frac{\alpha}{2}} &\approx (v^{\text{nom}})^\alpha + \\ &\frac{\alpha}{2} (v^{\text{nom}})^{\alpha-2} \left(v^{\text{nom}} e^{-j\phi} (v_k - v^{\text{nom}} e^{j\phi}) + v^{\text{nom}} e^{j\phi} (\bar{v}_k - v^{\text{nom}} e^{-j\phi}) \right) \end{aligned} \quad (41)$$

Then, simplifying (41), the following equation is obtained:

$$\begin{aligned} (v_k \bar{v}_k)^{\frac{\alpha}{2}} &= (v^{\text{nom}})^\alpha + \\ &\frac{\alpha}{2} (v^{\text{nom}})^{\alpha-2} \left(v^{\text{nom}} e^{-j\phi} v_k + v^{\text{nom}} e^{j\phi} \bar{v}_k - 2 (v^{\text{nom}})^2 \right) \end{aligned} \quad (42)$$

Therefore, (15) is replaced by the following affine equation:

$$S_{N_t}^{\text{load}} = S_{N_t}^{\text{ZIP}} \circ (M + H V_{N_t} + T \bar{V}_{N_t}) \quad (43)$$

where \circ represents the Hadamard product and M, H, T are constant vectors given by

$$M = \text{diag} (1 - \alpha) \quad (44)$$

$$H = \text{diag} \left(\frac{\alpha}{2 v^{\text{nom}} e^{j\phi}} \right) \quad (45)$$

$$T = \text{diag} \left(\frac{\alpha}{2 v^{\text{nom}} e^{-j\phi}} \right) \quad (46)$$

For the sake of completeness, the model with all the aforementioned approximations is presented in Table 3.

This model will be called Convex-TC in the following sections in order to differentiate from the NC-TC model. Notice that, the objective function includes a quadratic function with a positive definite matrix. This property is guaranteed if the hypergraph is connected. Therefore, the function is strongly convex, and this implies a global optimum and unique solution. In addition, the quadratic inequality constraints are also convex.

5.4. Operation under surplus energy limitation

Some grid codes prevent the sale of surpluses of energy. In these cases, the model must be limited with an additional constrain in order to prevent the power in the slack node becomes negative. The optimization model is modified in order to include this constraint as follows:

$$\begin{aligned} \min \quad &\sum_t c_t p_t^{\text{grid}} \\ &\text{real}(p_t^{\text{grid}}) \geq 0 \\ &\text{imag}(p_t^{\text{grid}}) \geq 0 \\ &+ \text{all constrains of Convex-TC} \end{aligned} \quad (47)$$

When the available energy is higher than the total load, the microgrid remains connected to the main grid, but the active and reactive power interchanged between the grid, and the microgrid is zero.

Table 3: Convex model for the tertiary control (Convex-TC)

Equation	Type	Modification
$\min \sum_t c_t p_t^{\text{grid}}$	objective function	affine
(38)	load flow	non-convex
(12)	power balance	affine
(13)	power loss	quadratic inequality
(14)	grid power	quadratic inequality
(43)	load model	affine
(16)	solar generation	affine
(17)	wind generation	affine
(18)	energy balance	affine
(19)	battery charging	quadratic inequality
(20)	battery discharge	quadratic inequality
(21)	battery power	affine
(22)	converter capacity	second-order cone
(23)	voltage limits	second-order cone
(24)	power deficit	affine
(25)	static reserve	affine

6. Results

6.1. CIGRE low voltage benchmark test system

A modified version of the benchmark test system for low-voltage microgrids proposed by CIGRE in [27] was initially used to illustrate the use of the model and its performance. This system is a 19-nodes, typical residential network with a peak power demand of 186.9 kW and a nominal voltage of 400V. The system was modified to include renewable generation and energy storage devices, as depicted in Fig 3.

The exponential model described in subsection 3.2 was used for the loads, with values of α given in Table 4. The system was analyzed for operation in 24h with intervals of 1h; a variable energy cost c_t was considered as shown in Figure 4.

Table 4: Loads description according to the exponential load model

Node	Peak power demand (W)	α
11	13400	2
13	47000	0
14	40000	2
18	70900	0
19	15600	1

Two main cases were analyzed, namely:

Case 1 (surplus sale): in this case, the slack node can inject and receive power from the microgrid; the optimization model decides the purchase or sale of energy, according to market prices and the generation and demand conditions of the microgrid.

Case 2 (without surplus sale): in this case, the slack node is limited to only supply power, i.e., the microgrid cannot inject power to the main grid. This type of limitation is due to some grid codes that are restrictive in terms of surplus sales.

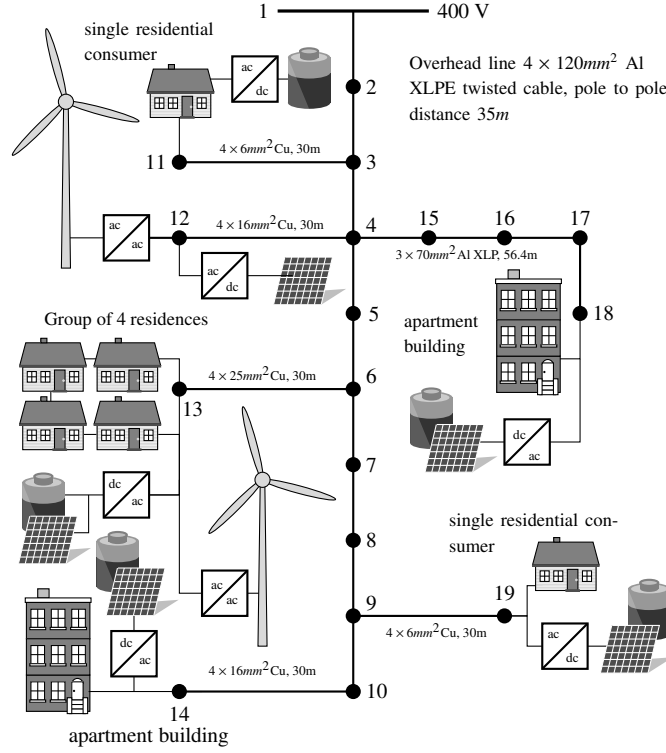


Figure 3: The CIGRE low voltage benchmark test system.

6.2. Case 1 (surplus sale)

The behavior of the TC for this case is shown in Fig 5, where p^{grid} is the power taken or sold to the main grid, and p^{ER} represents the power provided by the photovoltaic units, wind turbines, and batteries. As a result, the microgrid takes power from the main grid in periods where the renewable generation and batteries can not satisfy the load or when the energy has a low price. Eventually, the microgrid sold power to the system when the generator can supply the load, and there is an excess of generation.

The photovoltaic generation uses all its available resources, injecting the maximum amount of power that the irradiance profile allows in all the periods. The behavior of the photovoltaics units is represented in Fig 6.

Wind turbines have the same behavior as photovoltaic sources, as shown in Fig 7. These use the available wind speed profile, giving a result where the turbine can provide the maximum power in each period according to the wind speed forecast.

Finally, and considering an initial batteries SOC of 50%, these have a response to the load, as shown in Fig 8.

Notice that all batteries have similar behavior; they charge completely in periods of low prices, low demand and/or high generation, to discharge in periods with high demand when the prices are higher.

6.3. Case 2 (without surplus sale)

The power provided by the slack node is limited in all the periods of the tertiary control. This constraint is represented as follows:

$$p_t^{\text{grid}} \geq 0 \quad (48)$$

Therefore, renewable generation never overtakes the load demand, and the microgrid can not inject power into the main grid. In the periods that the demand exceeds the maximum renewable generation and the power that the batteries can provide, the main grid injects power to the microgrid to supply the loads, as shown in Fig 9.

The photovoltaic generation uses almost all of its available resources, limiting its generation in periods of maximum irradiance, as depicted in Fig 10. In this way, the microgrid keeps an equilibrium between generation and

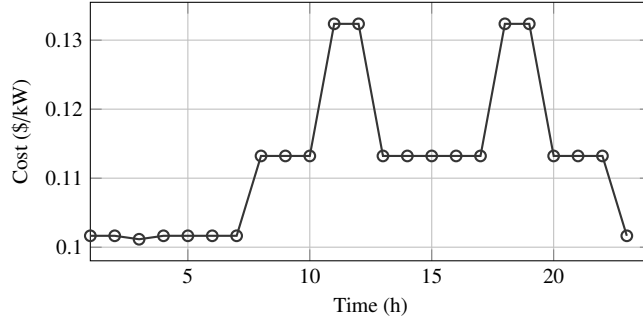


Figure 4: Prices from XM S.A.S, Colombian national interconnected system operator. Real time pricing for 24 consecutive hours in 2019.

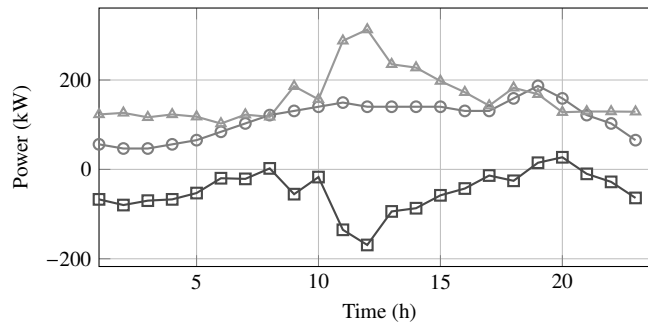


Figure 5: Tertiary control the slack node (\square), load demand (\circ) and power P_{ER} (\triangle) for the Case 1.

demand. Likewise, wind turbines reduce their generation to balance the load and generation. The behavior related to the wind turbines is shown in Fig 11.

Eventually, the SOC and the batteries' initial state is the same as in the previous case. The batteries tend to charge up when existing a surplus of power supplied by the generation, seizing all the resources. However, the batteries try to inject power to the microgrid to maintain the balance in periods that the load power overtakes the generation, as shown in Fig 12; in these periods, the tertiary control requires to minimize the purchase of energy to the main grid and reduce costs in the peak of demand.

6.4. Software implementation

All numerical experiments were performed in *CvxPy*, a domain-specific language for convex optimization embedded in Python [28]. This module allows to write the model in a natural optimization syntax and call free and/or commercial packages to solve the problem. Different solvers were used to comparing the model performance in terms of operative cost and execution time. Results are presented in Table 5, using a personal computer with 64-bit Operating system and processor Intel (R) Core (TM) i7-8700 CPU, 3.20 GHz, and 8GB of RAM.

Except for SCS, all solvers achieve the same optimal solution, although with different time calculations and number of iterations. The model achieves the same global solution as was expected for convex optimization models. Time calculation was less than 1s for the solvers in which the model achieves convergence. This performance is important because a tertiary control must be executed in real-time, with the architecture already depicted in Fig 1.

In practice, the optimization model is executed by a central controller that may be a personal computer or even a small single-board computer. Results presented in Table 5 demonstrate the proposed model is suitable for the former case. However, it is crucial to evaluate the model performance for a single-board computer.

In this work, a Raspberry-pi is proposed as a central controller; this is a low-cost small single-board computer used in industrial applications. The computation power of such a small device is much lower compared to a personal computer. However, it has some practical advantages, namely: the size of this board is 65mm x 30mm, so it can be integrated, for example, into the measurement unit of the microgrid; its cost is more than 20 times lower than a

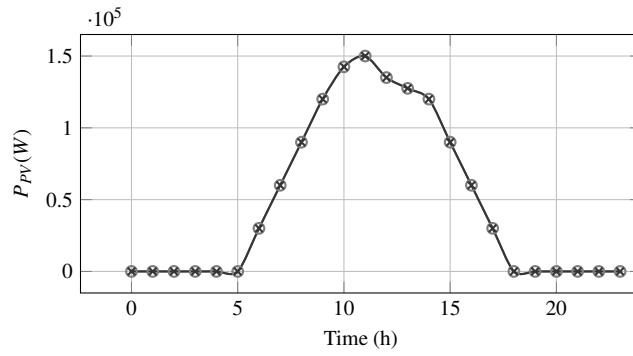


Figure 6: Optimal solar generation ($\rightarrow*$) and available solar generation ($\rightarrow\circ$) for the Case 1. The algorithm always takes the maximum solar generation.

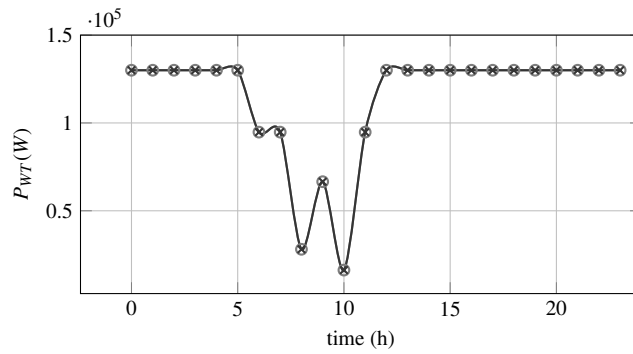


Figure 7: Optimal wind generation ($\rightarrow*$) and available wind generation ($\rightarrow\circ$) for Case 1. The algorithm always take the maximum available power.

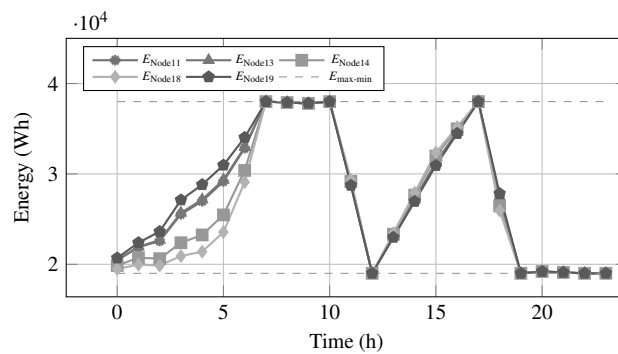


Figure 8: Energy stored in each battery for Case 1, considering the SOC of the batteries between 30% and 100% of the batteries energy.

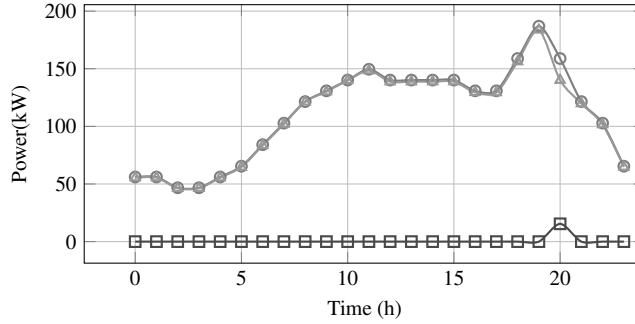


Figure 9: Energy exchange with the main grid (\square), total generation (\triangle) and total demand (\circ) for Case 2.

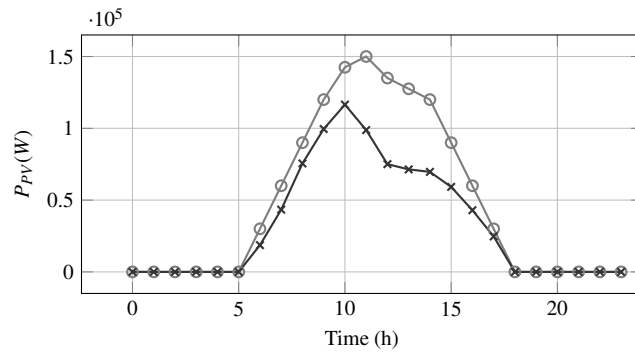


Figure 10: Optimal power generation (\times) and available power solar generation (\circ) for Case 2. The solar panels reduce their generation during the peak in order to maintain islanded operation.

personal or industrial computer; it does not have, nor does it require, additional elements such as graphic or sound cards; in general, it can be used as an embedded application for central control.

All simulations presented in Section 6 were executed again in a Raspberry-pi model BV 1.2 with a 1.2 GHz 64-bit quad-core processor, onboard 802.11n WiFi, Bluetooth, and USB boot capabilities. This board uses a Linux operative system and includes a Python interpreter. This Raspberry-pi allowed the installation of the module *CvxPy* for solving the optimization problems. The solver ECOS was used since this solver was explicitly designed for embedded applications [29]. For Case 1, the same results as Section 6 were obtained 24.6 seconds; for Case 2, the same results were obtained in 33.93 seconds. In both cases, the response of the convex-TC implementation was suitable for real-time requirements mentioned in section 2.

Table 5: Performance comparison between different solvers.

Case	Solver	Execution time (s)	Iterations	Operative cost (\$)	Status
Case I	Mosek	0.13	17	-146340.52	Optimal
	ECOS	0.19	33	-146340.52	Optimal
	ECOS BB	0.35	33	-146340.52	Optimal
	SCS	1.55	2560		Solved/Inaccurate
Case II	Mosek	0.32	36	7887.18	Optimal
	ECOS	0.12	21	7887.18	Optimal
	ECOS BB	0.18	21	7887.18	Optimal
	SCS	3.1	121		Solved/Inaccurate

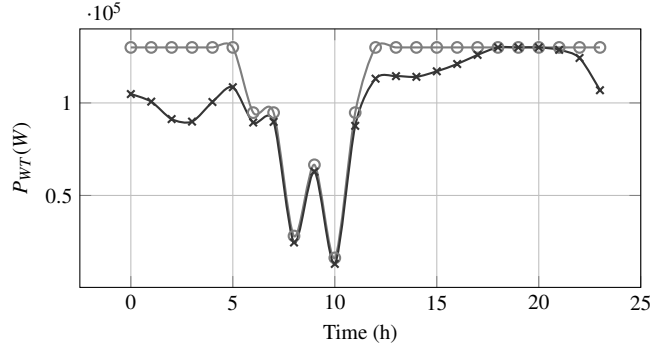


Figure 11: Optimal wind generation (\times) and available wind generation (\circ) for Case 2. The wind turbines reduce their generation maintaining the islanded operation and the balance between generation and power demand.

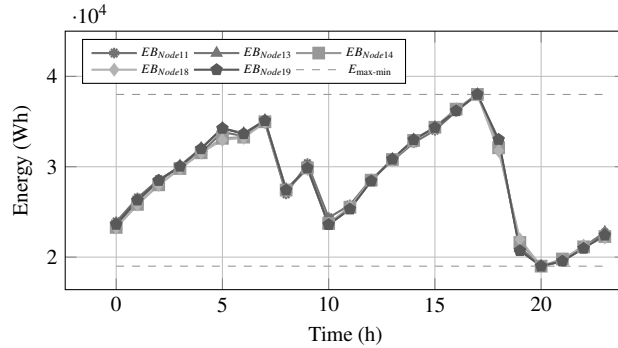


Figure 12: Energy stored in each battery for Case 2, considering the SOC of the batteries between 30% and 100% of the batteries energy.

6.5. Extension to power distribution networks

Although the proposed model was explicitly designed for microgrids, it may be extended to large power distribution systems; therefore, numerical experiments were performed in a modified version of the IEEE 123 node test feeder [30]. This model includes overhead and underground single-phase lines, capacitor banks, unbalanced loads with constant current, constant impedance, and constant power models. This test system was modified to include wind and solar energy and battery energy storage, as shown in Fig 13.

The proposed algorithm was executed under the same considerations as Case 1, using a personal computer with a 64-bit Operating system and processor Intel (R) Core (TM) i7-8700 CPU, 3.20 GHz, and 8GB of RAM. The model, in this case, consists of 197040 constraints, with 32736 convex cones and 196656 scalar variables. Despite its large size, the problem was solved in 2.26 seconds on average. Figure 14 shows the cycle of charge and discharge of battery energy storage devices. Results for each distributed resource are depicted in Fig 15.

7. Conclusions

In this paper, a convex optimization model for the tertiary control of unbalanced microgrids was proposed. This model considered 24h operation with unbalanced loads; Also, it considered a realistic model of the loads, renewable energy sources, and storage devices. A Wirtinger linearization was used for the power flow equations, the exponential model of the loads, and the quadratic model of the battery energy storage. The method was implemented under changing wind and solar energy penetration. The proposed methodology ensured the optimum operation of the microgrid components.

A real-time, low-cost, accurate implementation of the model was also considered. A Raspberry-pi was proposed as a central controller. The computation power of such a small device is much lower compared to a personal computer.

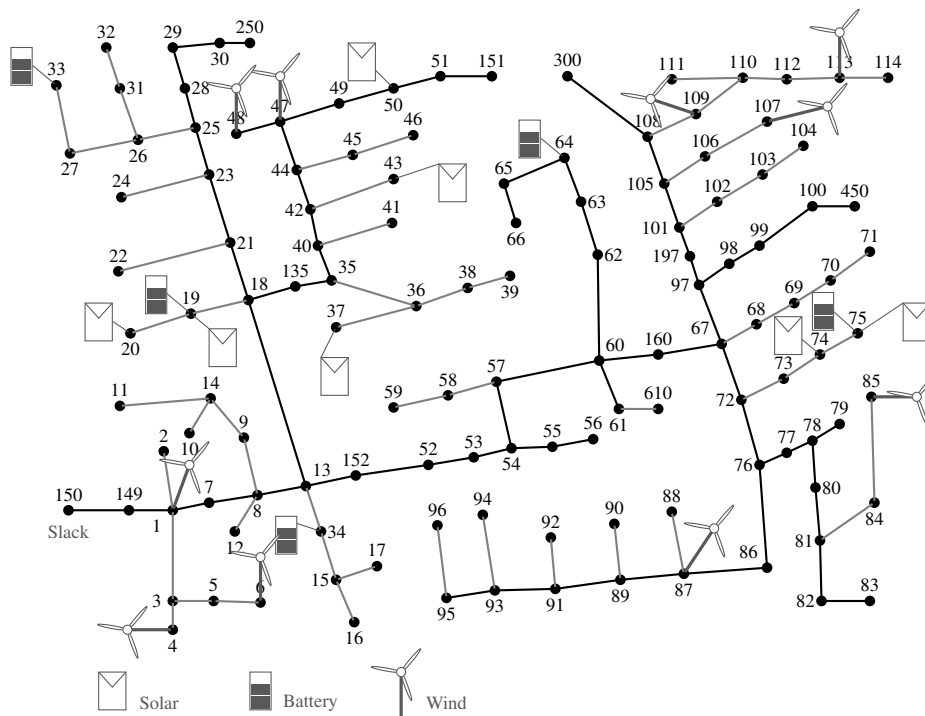


Figure 13: Modified IEEE123 test distribution system

However, the proposed model was executed successfully in this device. In this way, it was demonstrated the proposed model might be used for real-time operation. This implementation was a proof of concept under the worst-case scenario.

An intelligent predictor system based on prevision weather data (wind speed, solar irradiance, and temperature) has to be designed in further work. Prediction uncertainties on the renewable energies and load demand predictions have to be considered to design an autonomous system for an isolated area.

References

References

- [1] M. F. Zia, E. Elbouchikhi, M. Benbouzid, Microgrids energy management systems: A critical review on methods, solutions, and prospects, *Applied Energy* 222 (2018) 1033 – 1055. doi:<https://doi.org/10.1016/j.apenergy.2018.04.103>.

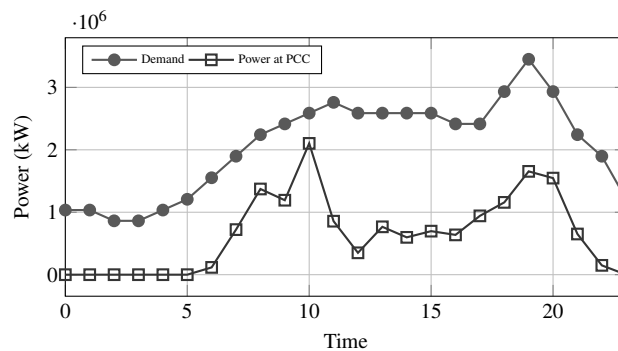


Figure 14: General results for the IEEE 123 node test system.

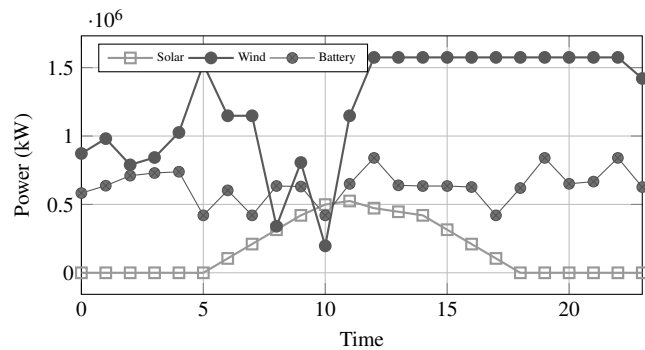


Figure 15: Total power generation for each distributed resource in the IEEE 123 node test system.

- URL <http://www.sciencedirect.com/science/article/pii/S0306261918306676>
- [2] F. Capitanescu, Critical review of recent advances and further developments needed in ac optimal power flow, *Electric Power Systems Research* 136 (2016) 57–68. doi:<https://doi.org/10.1016/j.epsr.2016.02.008>.
URL <http://www.sciencedirect.com/science/article/pii/S0378779616300141>
- [3] Y. Tang, K. Dvijotham, S. Low, Real-time optimal power flow, *IEEE Transactions on Smart Grid* 8 (6) (2017) 2963–2973. doi:10.1109/TSG.2017.2704922.
- [4] F. Delfino, G. Ferro, M. Robba, M. Rossi, An architecture for the optimal control of tertiary and secondary levels in small-size islanded microgrids, *International Journal of Electrical Power and Energy Systems* 103 (2018) 75–88. doi:<https://doi.org/10.1016/j.ijepes.2018.05.026>.
URL <http://www.sciencedirect.com/science/article/pii/S0142061517330090>
- [5] D. Y. Yamashita, I. Vechiu, J.-P. Gaubert, A review of hierarchical control for building microgrids, *Renewable and Sustainable Energy Reviews* 118 (2020) 109523. doi:<https://doi.org/10.1016/j.rser.2019.109523>.
URL <http://www.sciencedirect.com/science/article/pii/S1364032119307312>
- [6] F. Zohrizadeh, C. Jozs, M. Jin, R. Madani, J. Lavaei, S. Sojoudi, A survey on conic relaxations of optimal power flow problem, *European Journal of Operational Research* 287 (2) (2020) 391–409. doi:<https://doi.org/10.1016/j.ejor.2020.01.034>.
URL <http://www.sciencedirect.com/science/article/pii/S0377221720300552>
- [7] D. K. Molzahn, I. A. Hiskens, A survey of relaxations and approximations of the power flow equations, *Foundations and Trends® in Electric Energy Systems* 4 (1-2) (2019) 1–221. doi:10.1561/3100000012.
URL <http://dx.doi.org/10.1561/3100000012>
- [8] Z. Yuan, M. Paolone, Properties of convex optimal power flow model based on power loss relaxation, *Electric Power Systems Research* 186 (2020) 106414. doi:<https://doi.org/10.1016/j.epsr.2020.106414>.
URL <http://www.sciencedirect.com/science/article/pii/S0378779620302200>
- [9] L. Bobo, A. Venzke, S. Chatzivasileiadis, Second-order cone relaxations of the optimal power flow for active distribution grids: Comparison of methods, *International Journal of Electrical Power and Energy Systems* 127 (2021) 106625. doi:<https://doi.org/10.1016/j.ijepes.2020.106625>.
URL <http://www.sciencedirect.com/science/article/pii/S0142061520341703>
- [10] A. Venzke, S. Chatzivasileiadis, D. K. Molzahn, Inexact convex relaxations for ac optimal power flow: Towards ac feasibility, *Electric Power Systems Research* 187 (2020) 106480. doi:<https://doi.org/10.1016/j.epsr.2020.106480>.
URL <http://www.sciencedirect.com/science/article/pii/S0378779620302832>
- [11] S. Li, W. Gong, L. Wang, X. Yan, C. Hu, Optimal power flow by means of improved adaptive differential evolution, *Energy* 198 (2020) 117314. doi:<https://doi.org/10.1016/j.energy.2020.117314>.
URL <http://www.sciencedirect.com/science/article/pii/S0360544220304217>
- [12] Z. Deng, M. D. Rotaru, J. K. Sykulski, Kriging assisted surrogate evolutionary computation to solve optimal power flow problems, *IEEE Transactions on Power Systems* 35 (2) (2020) 831–839. doi:10.1109/TPWRS.2019.2936999.
- [13] K. Sørensen, Metaheuristics—the metaphor exposed, *International Transactions in Operational Research* 22 (1) (2015) 3–18. arXiv:<https://onlinelibrary.wiley.com/doi/pdf/10.1111/itor.12001>, doi:<https://doi.org/10.1111/itor.12001>.
URL <https://onlinelibrary.wiley.com/doi/abs/10.1111/itor.12001>
- [14] J. C. Bedoya, Y. Wang, C.-C. Liu, Distribution system resiliency under asynchronous information using reinforcement learning, *IEEE Transactions on Power Systems* (2021) 1–1doi:10.1109/TPWRS.2021.3056543.
- [15] W. Liu, P. Zhuang, H. Liang, J. Peng, Z. Huang, Distributed economic dispatch in microgrids based on cooperative reinforcement learning, *IEEE Transactions on Neural Networks and Learning Systems* 29 (6) (2018) 2192–2203.
- [16] A. Venzke, G. Qu, S. Low, S. Chatzivasileiadis, Learning optimal power flow: Worst-case guarantees for neural networks (2020). arXiv:2006.11029.
- [17] D. Groppi, A. Pfeifer, D. A. Garcia, G. Krajačić, N. Duic, A review on energy storage and demand side management solutions in smart energy islands, *Renewable and Sustainable Energy Reviews* 135 (2021) 110183. doi:<https://doi.org/10.1016/j.rser.2020.110183>.
URL <http://www.sciencedirect.com/science/article/pii/S1364032120304731>
- [18] D. Wang, J. Qiu, L. Reedman, K. Meng, L. L. Lai, Two-stage energy management for networked microgrids with high renewable penetration, *Applied Energy* 226 (2018) 39–48. doi:<https://doi.org/10.1016/j.apenergy.2018.05.112>.
URL <http://www.sciencedirect.com/science/article/pii/S0306261918308328>

- [19] P. Vergara, J. C. Lopez, M. J. Rider, H. R. Shaker, L. C. da Silva, B. N. Jorgensen, A stochastic programming model for the optimal operation of unbalanced three-phase islanded microgrids, *International Journal of Electrical Power and Energy Systems* 115 (2020) 105446. doi:<https://doi.org/10.1016/j.ijepes.2019.105446>. URL <http://www.sciencedirect.com/science/article/pii/S0142061519306234>
- [20] D. Ramirez, A. Garces, J. Mora-Florez, A wirtinger linearization for the power flow in microgrids, in: *IEEE General Meeting 2019, Atlanta, Georgia, August 2019, 2019*.
- [21] M. Saleh, Y. Esa, M. E. Hariri, A. Mohamed, Impact of information and communication technology limitations on microgrid operation, *Energies* 12 (15). doi:10.3390/en12152926. URL <https://www.mdpi.com/1996-1073/12/15/2926>
- [22] S. Lab, An1138: Zigbee mesh network performance, AN1138.
- [23] M. Bazrafshan, N. Gatsis, Comprehensive modeling of three-phase distribution systems via the bus admittance matrix, *IEEE Transactions on Power Systems* 33 (2) (2018) 2015–2029. doi:10.1109/TPWRS.2017.2728618.
- [24] SMA, Technical information for efficiency and derating of Sunny Boy storage, SMA, 2019.
- [25] R. Remmert, *Theory of Complex Functions*, 1st Edition, Vol. 1, Springer-Verlag, New York, 1989.
- [26] R. Hunger, An introduction to complex differentials and complex differentiability, technical report. URL <https://mediatum.ub.tum.de/doc/631019/631019.pdf>
- [27] S. Papanthassiou, N. Hatziaargyriou, K. Strunz, A benchmark low voltage microgrid network, *CIGRE Symposium*.
- [28] S. Diamond, S. Boyd, CVXPY: A Python-embedded modeling language for convex optimization, *Journal of Machine Learning Research* 17 (83) (2016) 1–5.
- [29] A. Domahidi, E. Chu, S. Boyd, Ecos: An socp solver for embedded systems, in: *2013 European Control Conference (ECC), 2013*, pp. 3071–3076. doi:10.23919/ECC.2013.6669541.
- [30] K. P. Schneider, B. A. Mather, B. C. Pal, C. . Ten, G. J. Shirek, H. Zhu, J. C. Fuller, J. L. R. Pereira, L. F. Ochoa, L. R. de Araujo, R. C. Dugan, S. Matthias, S. Paudyal, T. E. McDermott, W. Kersting, Analytic considerations and design basis for the IEEE distribution test feeders, *IEEE Transactions on Power Systems* 33 (3) (2018) 3181–3188. doi:10.1109/TPWRS.2017.2760011.

Founding

This research result is funded by UTP and the Colombian Science Ministry (Minciencias), project 111077657914, contract 031-2018, and project 321-2019.

Credit author statement

Diego-Alejandro Ramirez: methodology, software, writing. *Alejandro Garcés*: conceptualization, methodology, writing, validation. *Juan-José Mora-Flórez*: validation, writing, editing.

Declaration of Competing Interest

The authors declare that they have no known competing financial interests or personal relationships that could have appeared to influence the work reported in this paper.